1994ApJ...420..294B

THE ASTROPHYSICAL JOURNAL, 420:294–306, 1994 January 1
© 1994. The American Astronomical Society. All rights reserved. Printed in U.S.A.

PROTON AND ELECTRON MEAN FREE PATHS: THE PALMER CONSENSUS REVISITED

JOHN W. BIEBER, WILLIAM H. MATTHAEUS, AND CHARLES W. SMITH
Bartol Research Institute, University of Delaware, Newark, DE 19716
AND
WOLFGANG WANNER, MAY-BRITT KALLENRODE, AND GERD WIBBERENZ
Institut für Reine und Angewandte Kernphysik, Universität Kiel, Otto-Hahn-Platz 1, D-24118 Kiel, Germany
Received 1993 February 18; accepted 1993 July 13

ABSTRACT

We present experimental and theoretical evidence suggesting that the mean free path of cosmic-ray electrons and protons may be fundamentally different at low to intermediate (< 50 MV) rigidities. The experimental evidence is from *Helios* observations of solar energetic particles, which show that the mean free path of 1.4 MV electrons is often similar to that of 187 MV protons, even though proton mean free paths continue to decrease comparatively rapidly with decreasing rigidity down to the lowest channels (~100 MV) observed. The theoretical evidence is from computations of particle scattering in dynamical magnetic turbulence, which predict that electrons will have a larger mean free path than protons of the same rigidity. In light of these new results, "consensus" ideas about cosmic-ray mean free paths may require drastic revision.

Subject headings: cosmic rays — interplanetary medium — MHD — turbulence

1. INTRODUCTION

Understanding the mechanism by which energetic charged particles scatter in turbulent magnetic fields continues to be one of the foremost problems of modern cosmic-ray physics. This problem has been put in sharpest focus by observations of cosmic rays in the solar wind. Fitting cosmic-ray observations to diffusion models, especially in solar energetic particle events, has allowed us to determine representative values of the scattering mean free path and has given some indication of how the mean free path varies with particle rigidity (Palmer 1982). However, a satisfactory theory for deriving the observed mean free path from the known properties of turbulence in space is still lacking.

Early treatments of scattering theory employed quasi-linear approximations in a magnetostatic "slab" model (Jokipii 1966), in which the wavevectors of the turbulent fluctuations are aligned with the mean magnetic field. In an influential review article, Palmer (1982) compared the predictions of this model with observations and noted two major discrepancies. First, the observed mean free paths are generally larger than the theoretical prediction, with a typical discrepancy amounting to nearly a factor of 10 for 10 MeV protons. Second, the observations are broadly consistent with a rigidity-independent mean free path from 0.5 to 5000 MV, but the theory predicts that the mean free path should increase with increasing rigidity.

Subsequent investigations have explored particle scattering in geometries other than the axisymmetric slab model, including isotropic geometry (Hasselmann & Wibberenz 1968; Fisk et al. 1974; Kunstmann 1979) and oblique wave models (Lee & Völk 1975; Jones, Birmingham, & Kaiser 1978; Jaekel & Schlickeiser 1992). Within the context of resonant magnetostatic theory, such geometries generally yield reduced rates of scattering (compared with the slab model) and can even lead to infinite mean free paths.

There has been continuing interest in the mechanism by which particles scatter through 90° pitch angle. Recent work has shown that resonant scattering will be strongly damped near 90° owing to the unavoidable presence of dissipation processes at the small scales which govern the scattering rate in this regime (Davila & Scott 1984; Bieber, Smith, & Matthaeus 1988; Smith, Bieber, & Matthaeus 1990a). As a result, the mean free path is formally infinite (in resonant magnetostatic theory) regardless of the turbulence geometry assumed. This emphasizes anew the need to identify the dominant higher order process that allows the particles to scatter through 90° and yields a mean free path in agreement with observation. Among proposed mechanisms are "mirroring" by fluctuations of the magnetic field magnitude (Goldstein, Klimas, & Sandri 1975), a variety of nonlinear extensions of the theory (Owens 1974; Völk 1975; Goldstein 1976; Jones et al. 1978), wave propagation effects (Schlickeiser 1988, 1989; Schlickeiser, Dung, & Jaekel 1991), and effects of dynamical turbulence (Bieber & Matthaeus 1991, 1992).

The purpose of the present paper is to present new theoretical and observational evidence suggesting that "consensus" ideas about cosmic-ray mean free paths may require drastic revision. Specifically, we propose that proton and electron mean free paths may be fundamentally different at low to intermediate rigidities (< 50 MV) owing to an explicit speed dependence (beyond that inherent in any rigidity dependence) of the mean free path. Section 2 presents a critical review of observations and shows, in particular, that the observations underlying the Palmer consensus do not contravene the possibility of a fundamental difference between proton and electron transport. Section 3 presents two key *Helios* observations supportive of our hypothesis, and § 4 presents the new theoretical ideas that motivate our proposals. Our conclusions are summarized in § 5.

2. THE PALMER CONSENSUS REVISITED

Figure 1 presents our re-creation and extension of the Palmer (1982) consensus plot. Solid and open symbols denote, respectively, mean free paths derived from electron and proton observations. Circles in Figure 1 denote actual determinations of the mean free path, while upward-pointing triangles denote

© American Astronomical Society • Provided by the NASA Astrophysics Data System

1994ApJ...420..294B

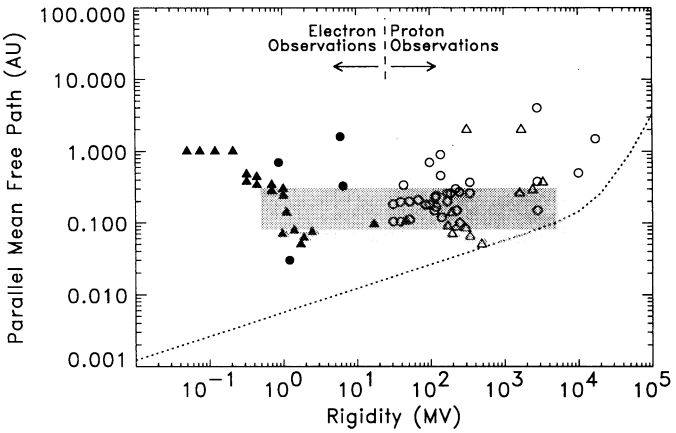

FIG. 1.—Cosmic-ray parallel mean free path vs. particle rigidity. Filled and open symbols denote results derived from electron and proton observations, respectively. See text for source references. Circles and upward-pointing triangles denote actual values and lower- limit values, respectively. The shaded band is the observational consensus enunciated by Palmer (1982). The dotted line represents the prediction of standard quasi-linear theory for magnetostatic, dissipationless turbulence with slab geometry (Jokipii 1966).

lower-limit values. In most cases the limit values are from studies that neglected possible extended injection near the Sun, due, for example, to coronal transport (Reid 1964; Axford 1965) or shock processes. Such processes augment interplanetary scattering to broaden the observed density profile of an event, and studies that ignore them generally underestimate the true mean free path. Palmer concluded that the empirical mean free paths could be characterized by a "consensus" band, shown shaded in Figure 1, which extends from 0.08 to 0.3 AU and spans a rigidity range of 0.5–5000 MV. The dotted line shows the prediction of conventional quasi-linear theory (Jokipii 1966) using the magnetostatic slab model. In deriving this prediction, we use the same representative interplanetary magnetic field spectrum (§ 4.3 below) that we will later employ in our computations of scattering in dynamical turbulence, except that we have omitted the dissipation range and thereby allowed the inertial range to extend to arbitrarily large wavenumbers.

In putting Figure 1 together, we have consulted the original sources of studies cited by Palmer (1982). Specifically, Figure 1 includes observations by Lin (1970, 1974), Palmer, Palmeira, & Allum (1975), Palmer et al. (1978), McCarthy & O'Gallagher (1976), Ford, Palmer, & Sanders (1977), Hamilton (1977), Schulze, Richter, & Wibberenz (1977), Zwickl & Webber (1977, 1978), Ma Sung & Earl (1978), Smart et al. (1979), Bieber et al. (1980), Chenette (1980), Debrunner & Lockwood (1980), Potter, Lin, & Anderson (1980), and Lockwood et al. (1982).

In addition, we have extended Palmer's compilation with some new mean free path determinations reported within the last 10 years. Specifically, these are Bieber & Pomerantz (1983), Kane, Evenson, & Meyer (1985), Bieber, Evenson, & Pomerantz (1986), Beeck et al. (1987), Dröge, Wibberenz, & Klecker (1990), Ruffolo (1991), and Chen & Bieber (1993). Two limit data points have been placed at 0.05 and 0.12 MV to represent Lin's (1985) observation that the transport of 2–15 keV electrons is essentially always scatter-free.

2.1. *Palmer Consensus: Standard Interpretation*

Figure 1 displays two well-known discrepancies between scattering theory and cosmic-ray observations: the predicted mean free paths are "too small" and have the "wrong" energy dependence (Wibberenz, Hasselmann, & Hasselmann 1970; Palmer 1982). Remarkably, not a single one of the 68 data points falls on or below the theoretical prediction shown by the dotted line. Recent studies of MeV protons in a large number of solar events likewise find this discrepancy in event-by-event comparisons of observed mean free paths with theoretical ones derived from magnetic spectra measured concurrently with the particle event (Wanner & Wibberenz 1993; Wanner et al. 1993). There is considerable variation among individual events, with observed mean free paths ranging from ~ 0.8 to ~ 50 times the theoretical value (Wanner et al. 1993). The clear tendency is still for the theoretical values to be too small.

The energy dependence exhibited by the theoretical curve in Figure 1 is related to the slope of the reduced power spectrum of the turbulence. With a spectrum varying as k^{-q}, where k is wavenumber, the mean free path is expected to vary as P^{2-q}, where P is particle rigidity. Because our model spectrum has a Kolmogorov ($k^{-5/3}$) inertial range, the predicted mean free path varies as $P^{1/3}$ for cosmic rays resonant with inertial range fluctuations. At very low wavenumbers, our model spectrum turns over (i.e., q decreases), which causes the rigidity dependence to steepen above ~ 10 GV.

In contrast, the observed mean free paths in Figure 1 show little tendency to decrease with decreasing rigidity. The shaded band shows Palmer's (1982) characterization of the observational "consensus." There is, indeed, a great deal of variation among individual events, and a substantial number of the data points are only lower-limit values. Nonetheless, the observations taken as a whole (and with no distinction made between proton and electron data) would seem to lend no support to the energy variation predicted by theory.

2.2. *A New Interpretation: Are Proton and Electron Mean Free Paths Fundamentally Different?*

Figure 1 also highlights an aspect of the Palmer consensus that is usually overlooked: electron and proton measurements contribute to entirely distinct rigidity ranges that do not (at present) overlap. Mean free paths below 25 MV are derived exclusively from electron observations, whereas those above 25 MV are derived exclusively from proton observations. It has been commonplace to ignore the distinction between electron and proton data, because in resonant magnetostatic scattering theory rigidity is the only property of the particle that influences the mean free path. (If the turbulence has finite magnetic helicity, the sign of the particle charge can also enter as a second-order effect [Bieber, Evenson, & Matthaeus 1987; Bieber & Burger 1990], but we will not consider such effects here.)

Pure rigidity dependence of the mean free path is closely tied to the magnetostatic approximation, however. Recent studies have relaxed this approximation by considering finite wave propagation speeds (Schlickeiser 1988, 1989; Schlickeiser, Dung, & Jaekel 1991; Achatz et al. 1993a, b) and by introducing a fully dynamical representation of the scattering turbulence (Bieber & Matthaeus 1991, 1992), an approach we will explore further in § 4 below. Both approaches predict that the mean free path has an explicit speed dependence, such that electrons have a different mean free path from protons of the same rigidity. The difference is largest at the lower rigidities, where such speed differences are most pronounced, and becomes vanishingly small at high rigidities, where both species are relativistic.

© American Astronomical Society • Provided by the NASA Astrophysics Data System

1994ApJ...420..294B

Turning again to Figure 1, we find nothing to contravene this possibility, but some significant alterations to the standard interpretation discussed above are implied. Although the problem with "too small" theoretical mean free paths remains, the conclusion of rigidity-independent mean free paths for both species is no longer compelling when the possibility of a fundamental difference between electron and proton scattering is admitted. Taken by themselves, in fact, the proton observations are compatible with a rigidity variation similar to the theoretical prediction (though at a higher level and with a great deal of scatter from event to event).

There are various indications, however, that electron mean free paths may indeed depart significantly from the theoretical prediction shown in Figure 1. One is Lin's (1985) observation that electrons with energies below 15 keV (i.e., rigidities below 0.12 MV) essentially always propagate scatter-free, whereas electrons with energies above 15 keV are often diffusive. It has also been suggested from analyses of individual solar particle events that electron mean free paths may decrease monotonically from 0.3 to 1.7 MV (Dröge et al. 1990). Finally, some aspects of the solar modulation of Galactic electrons are suggestive of a minimum electron mean free path between ~ 50 and ~ 500 MV (Evenson et al. 1979), with increasing mean free paths both below and above this range. We observe that such a minimum in the mean free path might crudely be described as "energy-independent" over a fairly broad energy range.

We will return to the issue of electron and proton mean free paths in § 4. We first present some key *Helios* observations which more sharply define observational constraints that an acceptable scattering theory must satisfy.

3. TWO KEY OBSERVATIONS FROM *Helios*

Although some of the scatter in Figure 1 may result from differing experimental and analytical methods, we believe most of the scatter is genuine and reflects a high degree of variability from event to event (Kunow et al. 1991). Thus, in seeking to understand and characterize proton and electron mean free paths, it is advantageous to compare results for different rigidities and species in the same solar particle event. Accordingly, this section discusses individual solar energetic particle events observed in the inner heliosphere by the Kiel cosmic-ray telescopes (Principal Investigator: H. Kunow) on board the spacecraft *Helios 1* and *Helios 2*. Two key results will be demonstrated: (1) that the mean free path of 1.4 MV electrons is often similar in magnitude to that of 187 MV protons, and (2) that ~ 100–300 MV proton mean free paths always increase with increasing rigidity when several energy channels can be analyzed in a single event.

3.1. *Transport Model*

In deducing particle mean free paths from observed time-intensity and time-anisotropy profiles of solar events, a basic assumption is that the particles are essentially injected close to or at the Sun (i.e., particles coming from interplanetary shocks are not included in discussing the events) and then propagate outward into the interplanetary medium. This propagation consists of the adiabatic motion in the smooth average interplanetary magnetic field combined with pitch-angle scattering due to the field irregularities (Roelof 1969). For sufficiently strong scattering the propagation can be modeled by a process of spatial diffusion. Depending on the relative importance of convection with the solar wind and spatial diffusion, one may also have to take adiabatic deceleration into account (Parker 1965). Before performing a fit to observed particle data, it is therefore important to estimate the relative size of the competing effects in order to select the proper transport model. In short, one can state that for weak scattering (large mean free path) one may neglect convective processes and use only the combined effects of focusing and pitch-angle scattering. Numerical solutions for this type of transport are given by Ng & Wong (1979). In contrast, for strong scattering (small mean free path) adiabatic focusing can be neglected, but convective processes must be considered. Numerical solutions for this situation have been given, e.g., by Hamilton (1977).

It is well known that a finite length of injection of particles close to the Sun leads to an extended time profile for an observer in space. In order to separate this effect from similarly long-lasting intensity profiles caused by a small mean free path, one has to fit intensity and anisotropy data simultaneously. Let us discuss as an example in Figure 2 the event of 1980 March 25, based on data observed on *Helios 1* at a positon of 0.91 AU (similar arguments apply to the other events discussed in this work). The example also serves to demonstrate the range of parameters which gives a reasonable fit to the data.

To fit this event, we employ numerical solutions of the equation of focused transport, as appropriate for relatively weak scattering (Ng & Wong 1979; Schlüter 1985). The intensity of scattering between the Sun and the observer is characterized by a radial mean free path λ_r, which we take to be independent of heliocentric distance. See Kallenrode, Wibberenz, & Hucke (1992) for further discussion of this approach and the validity of mean free paths derived by it.

Electron observations at a rigidity of 1.4 MV, shown in the left-hand panel of Figure 2, are consistent with a radial mean free path of 0.2 AU. Proton observations at a rigidity of 187 MV, shown in the right-hand panel, lead to a radial mean free path of 0.25 AU. Only small deviations from these values in either direction can be allowed before the fits become unacceptable (see dashed lines in the right-hand panel of Figure 2 as an illustration). Obviously, the proton mean free path is only a factor of 1.25 larger than the electron mean free path, despite the large difference in rigidity.

These results also show that the propagation certainly cannot be characterized as scatter-free. Such a concept of essentially scatter-free transport has recently been suggested as an explanation for the relatively short intensity bursts of ^{3}He-rich impulsive solar events (Mason et al. 1989). It cannot be excluded that at certain times the level of magnetic turbulence is sufficiently low to lead to conditions of very weak scattering (Kunow et al. 1991; Wanner & Wibberenz 1993). Large variations of the turbulence level necessitate careful study of each individual event. The data in Figure 2, however, are not consistent with scatter-free transport. It would require an anisotropy which stays at high levels for a long period of time instead of the relatively fast decay observed, which is characteristic of a short injection at the Sun and subsequent diffusive transport.

Since particles propagate anisotropically along the average magnetic field, one has to convert λ_r to the parallel mean free path along the field via $\lambda_{\parallel} = \lambda_r/\cos^2 \psi$, where ψ is the angle between the average magnetic field and the radial direction. We take ψ to be the expected Parker spiral angle based upon the measured solar wind speed. It is this parallel mean free path to which we compare the predictions of scattering theory.

© American Astronomical Society • Provided by the NASA Astrophysics Data System

1994ApJ...420..294B

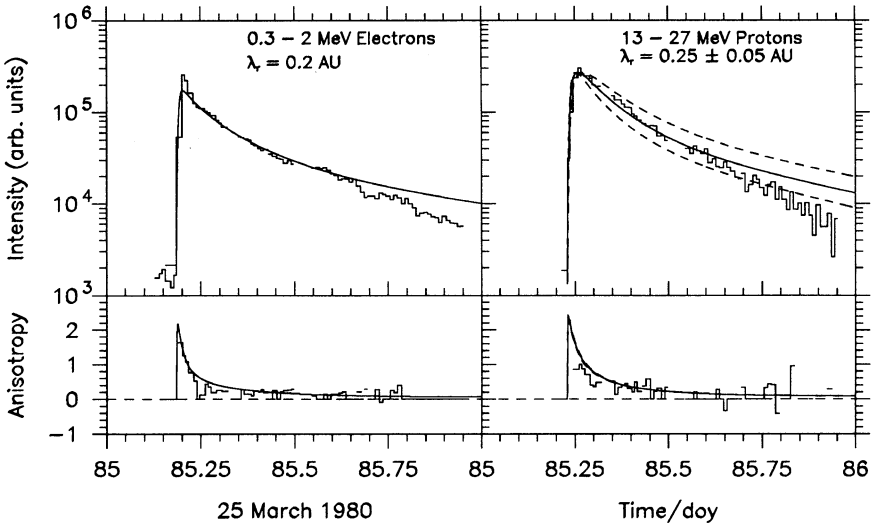

FIG. 2.—Illustration of fitting to a solar flare event using *Helios 1* observations on 1980 March 25 (day 85). The 0.3 to ~2 MeV electrons (*left-hand side*) can be fitted in intensity (*upper panels*) and anisotropy (*lower panels*) using a radial mean free path of approximately the same size (0.2 AU) as that for the 13–27 MeV protons (0.25 AU; *right-hand side*). Dashed lines in the upper right-hand panel demonstrate that even small alterations of the mean free path (by ±0.05 AU) produce unacceptable fits. Extended injection of particles at the Sun was assumed.

3.2. 1.4 MV *Electrons Compared with* 187 MV *Protons*

Mean free paths of particles can vary considerably from one event to the other, as is evident from Figure 1. As a consequence, a comparison of electron and proton mean free paths must be made on an event-by-event basis. We have done this for 11 *Helios* events for which a mean free path could be deduced from both proton and electron channels. Proton results are derived mostly from the *Helios* 13–27 MeV energy channel, which has an average rigidity of 187 MV. In three cases the neighboring 4–13 MeV channel was used, but this is acceptable, since mean free paths in this channel are only a factor of 1.2 smaller than in the 13–27 MeV channel assuming a typical rigidity dependence. Electron results are derived from the *Helios* 0.3 to ~2 MeV energy channel, which has an average rigidity of 1.4 MV.

Concurrent proton and electron mean free paths are available from *Helios 2* observations on 1976 March 28 (Bieber et al. 1980) and 1978 April 11 (Valdés-Galicia et al. 1988; Kallenrode et al. 1992); from *Helios 1* observations on 1978 April 8 (Beeck & Wibberenz 1986); and from both *Helios 1* and *Helios 2* on 1977 December 27 and 1978 January 1 (Wibberenz et al. 1989). Details of these events and the techniques used in deriving mean free paths are found in the references given. An additional four events are included from recent work of Kallenrode (1993). These are the events of 1980 March 25, 1981 January 14, 1981 May 5, and 1981 November 19, all observed on *Helios 1*. The model used for fitting is the one described earlier (§ 3.1) in the discussion of the event of 1980 March 25.

Results appear in Figure 3, which plots mean free paths of 1.4 MV electrons against those of 187 MV protons observed in the same event. The mean free path varies by a factor of 40, but individual points vary by little more than a factor of 2 from the dotted line, which indicates where the electron mean free path is exactly half the proton mean free path. Thus there is a close connection between the proton and electron scattering for individual events over a considerable range of mean free paths, noted also by Kunow et al. (1991). Five of the events have approximately the same mean free paths for electrons and protons. The ratio of electron to proton mean free paths ranges from 0.3 to 1.3, and the geometric mean of the 11 events is 0.56.

This should be compared with what is expected from conventional scattering theory. A slope of $q = 5/3$ for the inertial range in slab geometry would imply a mean free path varying as $P^{1/3}$ and, hence, a ratio of 0.20 for the two rigidities discussed here, not 0.56 as observed. This clearly shows that electron mean free paths do not follow the law established by conventional theory.

3.3. *Rigidity Dependence of Proton Mean Free Path*

The rough equality of 1.4 MV electron and 187 MV proton mean free paths could imply that cosmic-ray mean free paths are essentially independent of rigidity. We will now demonstrate the contrary by showing that ~100–300 MV proton mean free paths clearly and persistently increase with rigidity.

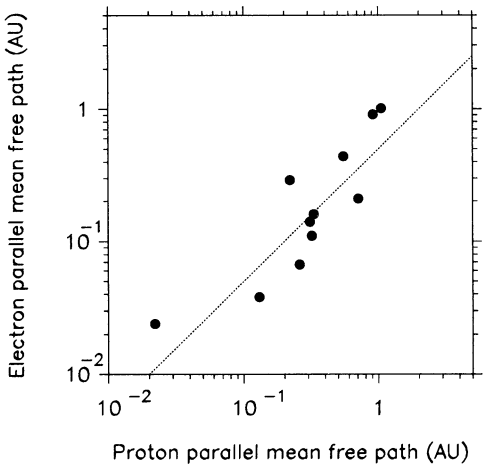

FIG. 3.—Scatter plot of parallel mean free paths of 1.4 MV electrons vs. those of 187 MV protons (except in three instances where a neighboring proton energy channel was used). The dotted line corresponds to an electron mean free path that is exactly half the proton mean free path. See text for source references.

© American Astronomical Society • Provided by the NASA Astrophysics Data System

1994ApJ...420..294B

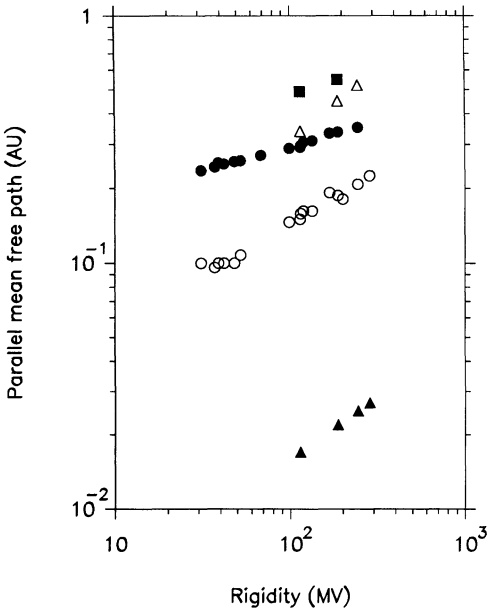

FIG. 4.—Proton parallel mean free path as a function of rigidity for several solar events. See text for source references.

Figure 4 presents proton parallel mean free paths versus rigidity for five events where two or more energy channels could be evaluated. The two most prominent events are those of 1977 November 22 and 1977 December 27, which are taken from Beeck et al. (1987). This study made use of data from the *Helios*, *ISEE 1* and *Voyager 1* space probes; the results displayed are for a heliocentric distance of 1 AU. The smallest mean free paths are for the event of 1978 April 11, which was analyzed in four *Helios* proton channels by Valdés-Galicia et al. (1988). Two additional events are from Kallenrode (1993). They were observed on 1980 March 25 by *Helios 1* (analyzed in two channels) and on 1979 June 9 by *Helios 2* (three channels).

All events clearly show an increase of the proton mean free path with rigidity. The slope of the events of 1977 November 22 and 1977 December 27 were given as 0.45 and 0.20, respectively. The slope for the event of 1978 April 11 is 0.53; for the event of 1980 March 25 it is 0.23; and for that of 1979 June 9 it is 0.56.

From these observations we conclude that protons show a rigidity variation that is considerably stronger than that suggested by a comparison of 1.4 MV electrons with 187 MV protons. Wanner & Wibberenz (1993) have argued that the proton result is not in contradiction with the observation of Palmer (1982) that all proton results taken together give a broad band of mean free paths that appears to be independent of rigidity. Most events in the database assembled by Palmer were evaluated at only one or very few rigidities, and mean free paths vary considerably from one event to the other. These two effects combine to obscure the rigidity dependence of proton mean free paths which is clearly evident when individual events are considered separately.

4. NEW THEORETICAL RESULTS: SCATTERING IN DYNAMICAL TURBULENCE

In this section we first describe how dynamical turbulence may be suitably represented. We then employ the slab model to illustrate how scattering theory is generalized from the magnetostatic to a fully dynamical representation. Next we present predicted mean free paths for protons and electrons, paying close attention to predictions of theory in relation to the *Helios* observational constraints developed in the preceding section. We employ slab geometry initially, using two alternative possibilities for the dynamical correlation function, and we conclude by showing some results from a composite slab/two-dimensional geometry.

4.1. *Dynamical Turbulence*

In the perspective of scattering theory, dynamical magnetic turbulence is most conveniently characterized by its two-point, two-time correlation function and related transforms of this function. Since we are restricting our discussion to the slab model, we need consider only one spatial dimension. Hence the correlation can be represented as $R_{xx}(z, t)$, where x represents one of the directions normal to the mean magnetic field, z is the spatial lag parallel to the mean field, and t is the lag time. In the axisymmetric slab model $R_{yy} = R_{xx}$, and $R_{zz} = 0$. We also neglect magnetic helicity, so that all the off-diagonal elements of the correlation matrix are zero.

Inclusion of an explicit lag-time dependence is how we represent the dynamical character of turbulence. We will generally discuss the turbulence power spectrum in terms of a Fourier transform of the correlation function with respect to its spatial coordinate but not its time coordinate, i.e.,

$$P_{xx}(k_z, t) = \frac{1}{2\pi}\int_{-\infty}^{+\infty} R_{xx}(z, t)e^{-ik_z z}dz \,. \quad (1)$$

To isolate more clearly the dynamical component of the turbulence spectrum, we define the "dynamical correlation function" $\Gamma(k_z, t)$ as follows:

$$P_{xx}(k_z, t) = P_{xx}(k_z, 0)\Gamma(k_z, t) \,. \quad (2)$$

This definition assumes that Γ does not depend upon the tensor indices i and j. However, this assumption can easily be relaxed if warranted by future studies of dynamical turbulence.

We shall also find it convenient to relate some aspects of particle scattering to the "Eulerian frequency spectrum," which is the Fourier transform of $R_{xx}(z, t)$ with respect to time at a spatial lag of zero,

$$G_E(\omega) = \frac{1}{2\pi}\int_{-\infty}^{+\infty} R_{xx}(0, t)e^{-i\omega t}dt \,. \quad (3)$$

For homogeneous, stationary turbulence, the symmetry property $R_{xx}(-z, -t) = R_{xx}(z, t)$ is satisfied, which in turn implies $G_E(-\omega) = G_E(\omega)$. As employed here, the Eulerian frequency spectrum is to be measured in the rest frame of the plasma. It is therefore entirely distinct from the frequency spectrum that results from sweeping of spatial variations past a stationary observer by bulk flow of the plasma.

We shall discuss in some detail two separate models for the dynamical correlation function:

$$\Gamma(k_z, t) = \exp(-\alpha|k_z|V_A|t|) \quad \text{(damping model)} \,, \quad (4)$$

$$\Gamma(k_z, t) = \exp(-\alpha^2 k_z^2 V_A^2 t^2) \quad \text{(random sweeping model)} \quad (5)$$

Here V_A is the Alfvén speed, and α is a parameter which allows us to adjust the strength of the dynamical effects, ranging from $\alpha = 0$ (magnetostatic limit) to $\alpha = 1$ (strongly dynamical). In

© American Astronomical Society • Provided by the NASA Astrophysics Data System

1994ApJ...420..294B

the present study we will consider only $\alpha = 1$, and we will adopt $V_A = 33.5$ km s^{-1}, a value representative of the solar wind at 1 AU. The reciprocal timescale $(\alpha | k_z | V_A)$ that appears in equations (4) and (5) is a parameterization that permits several types of physical timescales to be included in the models for temporal decorrelation. A value $\alpha \approx 1$ may signify decorrelation effects that take place at an Alfvénic timescale. If α is interpreted as $\delta B/B_0$ (ratio of fluctuating to mean magnetic field), the relevant timescale becomes comparable to the eddy turnover time. Letting α depend on parameters such as the plasma β (ratio of thermal to magnetic pressure) would permit inclusion of decorrelation effects associated with plasma waves (Schlickeiser & Achatz 1993). Apart from the issue of the choice of decorrelation timescales, the functional forms of the models represented in equations (4) and (5) can also be motivated reasonably well from turbulence theory.

The damping model was introduced in our preliminary studies of scattering in dynamical turbulence (Bieber & Matthaeus 1991, 1992). It has an exponential form of Γ, as appropriate for a damping process in which the correlation function of a monochromatic wave with wavenumber $|k_z|$ decays exponentially with a time constant of $(\alpha | k_z | V_A)^{-1}$. A detailed theoretical motivation for the damping model is currently under development. It has intuitive appeal, based on the idea that structures at a fixed scale suffer temporal distortions at a fixed rate. For purposes of modeling, this rate can be chosen, in accordance with the above discussion of the parameter α, to be associated with random wave propagation. Perhaps more significantly, the decay rate can be taken to be an approximation to the Kolmogorov decay rate for the appropriate scale. In either case the rate of decay will depend upon the parameterized speed αV_A and upon wavenumber. In slab geometry the only available wavenumber is $|k_z|$, but it may be useful in other geometries to consider models that depend on the full wavenumber magnitude as well.

The random sweeping model of dynamical turbulence has a Gaussian form of Γ. According to the random sweeping hypothesis (Tennekes 1975), the Eulerian frequency spectrum of turbulence is determined primarily by sweeping of small-scale spatial variations past the observer by the random motions of the larger scale eddies (as distinct from sweeping by an organized plasma flow or wind). Although not universally accepted (Yakhot, Orszag, & She 1989), the random sweeping model has found considerable support in the recent turbulence literature (Chen & Kraichnan 1989; Nelkin & Tabor 1990). Sanada & Shanmugasundaram (1992), in particular, discuss their numerical simulations in terms of a dynamical correlation function like the one defined here and conclude that a Gaussian form best describes their results.

A fully self-consistent representation of dynamical turbulence should in principle include a description of turbulent electric fields. The effect of electric fields on particle scattering and acceleration is conveniently expressed in terms of the electric field power spectrum and cross-spectra of the electric and magnetic fields (Schlickeiser & Achatz 1993). Evaluating the contribution of electric fields to particle scattering is difficult at this stage, however, because turbulence theory descriptions of the fluctuating electric field are much less well developed than turbulence theory descriptions of the fluctuating magnetic field.

Most existing treatments of the nature of turbulent electric fields are confined to statements made in the context of "mean field electrodynamics," a term ordinarily associated with various approximations adopted in dynamo theory (Moffatt 1978; Krause & Rädler 1980; Zel'dovich, Ruzmaikin, & Sokoloff 1983). In this approach the quantity of interest is usually the mean electric field (defined as a volume or time average over a relevant scale such as a correlation scale). Moreover, the mean electric field is typically eliminated in favor of some other property of the turbulence, such as the kinetic or magnetic helicity. However, such approaches say little about the spectrum of the induced electric field. It is this spectrum (or its associated correlation function) that would be needed to incorporate electric field effects in quasi-linear treatments of charged particle scattering.

Consequently, substantial new information on turbulence phenomenology is required before a complete formulation of particle scattering in dynamical turbulence can be constructed. Such a theory would need to include both direct effects of the electric field, as represented by models of the electric field correlation function and electric-magnetic cross-correlations, as well as indirect influences associated with temporal decay of the magnetic field correlation function. However important the direct effects may turn out to be, they are beyond the scope of this work, and we have restricted the present effort to extending earlier theories by considering only the temporal decorrelation effect, while continuing to ignore whatever direct electric field effects may occur.

4.2. *Scattering Theory*

The mean free path of cosmic-ray scattering parallel to the mean magnetic field, $\lambda_\parallel$, may be computed from the Fokker-Planck coefficient for pitch-angle scattering, $\Phi(\mu)$:

$$\lambda_\parallel = \frac{3}{2} V \int_0^1 \frac{(1-\mu^2)^2}{\Phi(\mu)} d\mu , \tag{6}$$

where V is the particle speed and μ is the cosine of the particle pitch angle (Jokipii 1966, Hasselmann & Wibberenz 1968, 1970; Earl 1974). Spatial scattering is often equivalently characterized by a diffusion coefficient, $K_\parallel \equiv \lambda_\parallel V/3$. Equation (6) makes use of the property that Φ is an even function of μ for turbulence lacking magnetic helicity. Note that some authors (e.g., Schlickeiser 1989) prefer to discuss pitch-angle scattering in terms of a phase-space diffusion coefficient $D_{\mu\mu}$, which is half the Fokker-Planck coefficient (i.e., $D_{\mu\mu} = \Phi/2$).

The Fokker-Planck coefficient for scattering in dynamical turbulence with slab geometry may in turn be computed from the correlation function of the magnetic field,

$$\Phi(\mu) = \frac{\Omega^2}{B_0^2} (1-\mu^2) \int_{-\infty}^{+\infty} R_{xx}(\mu V t, t) \cos(\Omega t) dt , \tag{7}$$

where Ω is the gyrofrequency of the particle and B_0 is the magnitude of the mean magnetic field. The only difference between this and the magnetostatic slab result (Jokipii 1966) is the presence of the second argument t of the correlation function. As we shall see, this seemingly minor alteration has far-reaching consequences for low- and moderate-energy cosmic rays.

Equation (7) may be recast in terms of the power spectrum, using equation (2) together with the inverse transform of equation (1),

$$\Phi(\mu) = \frac{\Omega^2}{B_0^2} (1-\mu^2) \int_{-\infty}^{+\infty} P_{xx}(k_z, 0) D(k_z) dk_z , \tag{8}$$

© American Astronomical Society • Provided by the NASA Astrophysics Data System

1994ApJ...420..294B

where the resonance function $D(k_z)$ depends upon the dynamical correlation function:

$$D(k_z) = \int_{-\infty}^{+\infty} \exp\,[i(k_z \mu V - \Omega)t]\Gamma(k_z, t)dt\ . \quad (9)$$

The magnetostatic limit of scattering theory can be recovered by setting $\Gamma = 1$. The resonance function is then a Dirac delta function centered on the resonant wavenumber of the particle, $k_{res} = \Omega/(\mu V)$. The scattering rate is determined by the power spectrum evaluated at this resonant wavenumber. Choosing instead an oscillatory form, $\Gamma = \cos\,(k_z V_A t)$, allows us to recover a specialized form of the Alfvén wave result proposed by Schlickeiser (1988, 1989). In this case the resonance function $D(k_z)$ becomes a pair of delta functions with sharp resonances at $k_{res} = \Omega/(\mu V \pm V_A)$.

We turn now to the dynamical correlation functions discussed in § 4.1. The two models of $\Gamma(k_z, t)$ shown in equations (4) and (5) yield two different forms of resonance function.

Damping model:

$$D(k_z) = \frac{2}{|\mu| V} \frac{(\alpha |k_z| V_A)/(|\mu| V)}{[(\alpha k_z V_A)/(|\mu| V)]^2 + [k_z - \Omega/(\mu V)]^2}\ , \quad (10)$$

Random sweeping model:

$$D(k_z) = \frac{\pi^{1/2}}{\alpha |k_z| V_A} \exp\left\{ - \frac{[k_z - \Omega/(\mu V)]^2}{4\alpha^2 k_z^2 V_A^2/(\mu^2 V^2)} \right\}. \quad (11)$$

The damping model as originally discussed by Bieber & Matthaeus (1991) presumed α to be of order 0.1–1 based on analogy with spectral theories (e.g., Matthaeus & Zhou 1989). Alternatively, if α is set to the ratio of the plasma thermal speed to the Alfvén speed, then the resonance given by equation (10) reduces to a form similar to that derived by Schlickeiser & Achatz (1993) for particle scattering by thermally damped plasma waves.

Both of the above two forms of resonance functions are now broadened resonances with a finite width determined by the value of $(\alpha |k_z| V_A)/(|\mu| V)$. We can recover the magnetostatic limit by letting $(\alpha |k_z| V_A)/(|\mu| V) \to 0$, in which case both resonance functions approach a delta function with resonance at $k_{res} = \Omega/(\mu V)$. However, this limit becomes unreachable for particle pitch angles sufficiently close to 90° ($\mu \to 0$). In this regime magnetostatic theory becomes inapplicable, and dynamical effects become the dominant factor governing the scattering rate.

We close this subsection by noting a remarkable relationship between the Eulerian frequency spectrum and the scattering rate at 90° pitch angle. (The relationship is exact only in the slab model, but qualitatively similar relationships govern other geometries.) Comparing equation (7) with μ set to zero with the definition of the Eulerian frequency spectrum given by equation (3), we find

$$\Phi(0) = \frac{2\pi\Omega^2}{B_0^2} G_E(\Omega)\ , \quad (12)$$

where we have used the symmetry relation $G_E(-\Omega) = G_E(\Omega)$. This attractively simple relationship asserts that the scattering rate at 90° is determined by the Eulerian frequency spectrum evaluated at the gyrofrequency of the particle. As we shall demonstrate shortly, this is a key result for understanding how dynamical turbulence affects particle scattering and leads to a fundamental difference in the mean free paths of low-energy protons and electrons.

4.3. *Model Spectrum*

As shown by equation (2), the full dynamical spectrum depends not only on the dynamical correction function $\Gamma(k_z, t)$ but also upon the function $P_{xx}(k_z, 0)$, which we will call the "magnetostatic limit" of the spectrum. Because we wish to provide realistic illustrations of the scattering theory proposed here, we have taken care to construct a model spectrum that is consistent with the average observed properties of interplanetary magnetic turbulence. For the magnetostatic limit of the spectrum we employ a functional form

$$P_{xx}(k_z, 0) = \begin{cases} 2\pi C\lambda(1 + k_z^2 \lambda^2)^{-5/6}\ , & \text{for } |k_z| < k_d\ , \\ 2\pi C\lambda(1 + k_d^2 \lambda^2)^{-5/6}(|k_z|/k_d)^{-3}\ , & \text{for } |k_z| \geq k_d\ , \end{cases} \quad (13)$$

where the index $-\frac{5}{6}$ has been chosen to yield a Kolmogorov ($|k_z|^{-5/3}$) inertial range consistent with observation (e.g., Wanner & Wibberenz 1991).

As illustrated in Figure 5, the parameters C and λ were selected to produce a model spectrum consistent with representative interplanetary magnetic spectra as derived from survey observations acquired over multiyear periods. For the low-frequency fluctuations, we were guided by survey results of Hedgecock (1975; *dotted line*) and Bieber et al. (1993; *dashed line*). For the inertial range fluctuations, we targeted the 1 AU end of regressions obtained by Wanner & Wibberenz (1991; *dot-dash line*). As Figure 5 demonstrates, the choices $C = 0.5$ nT^2 and $\lambda = 4.55 \times 10^9$ m produce a model spectrum (*solid line*) in reasonable agreement with these diverse observational studies. This choice of C and λ implies that the total variance in one perpendicular component of the field is 13.2 nT^2, and the

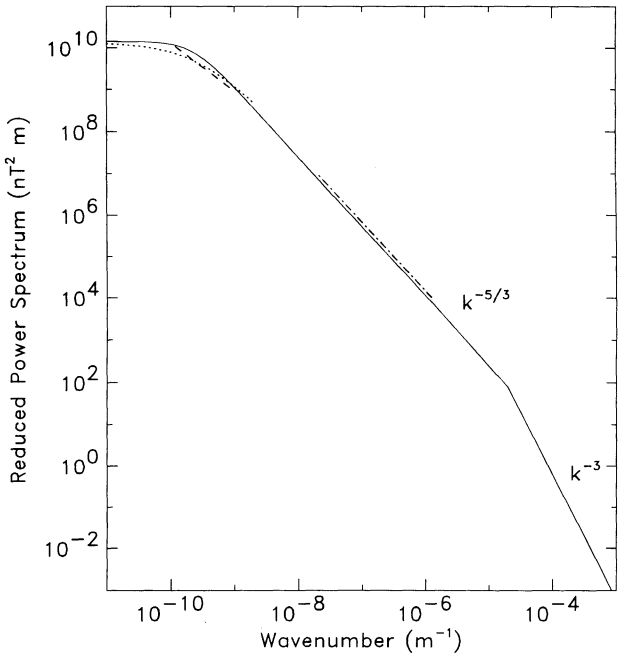

FIG. 5.—Reduced perpendicular power spectrum of slab model used in our scattering theory computations (*solid line*) compared with survey observations by Hedgecock (1975; *dotted line*), Bieber et al. (1993; *dashed line*), and Wanner & Wibberenz (1991; *dot-dash line*).

© American Astronomical Society • Provided by the NASA Astrophysics Data System

1994ApJ...420..294B

correlation length of the turbulence is 3.4×10^9 m (0.023 AU), which is consistent with survey results of Matthaeus, Goldstein, & King (1986). We note that all of the observational results are based on frequency spectra which have been converted to wavenumber spectra by means of the Taylor frozen-in flow approximation together with the assumption of slab geometry. (See Bieber et al. 1993 for details.) In addition, the Hedgecock and Wanner & Wibberenz results have been divided by 2 to convert them to "two-sided" spectra (defined for negative as well as positive wavenumbers) in conformance with the convention implied by equation (1).

Also depicted in Figure 5 is the sharp break between inertial and dissipation ranges at wavenumber $|k_z| = k_d$. Dissipation range behavior is generally observed above spacecraft frame frequencies ~ 1 Hz (Coroniti et al. 1982; Denskat, Beinroth, & Neubauer 1983; Smith, Matthaeus, & Ness 1990b). Accordingly, we have chosen $k_d = 2 \times 10^{-5}$ m^{-1} for our model spectrum as appropriate for slab geometry with a solar wind speed of 445 km s^{-1}. Observations also suggest that the spectrum above 1 Hz follows a power-law frequency dependence with reported indices ranging from -2.3 to -5.3 (Coroniti et al. 1982; Denskat et al. 1983; Smith et al. 1990b). However, we know on theoretical grounds that the wavenumber spectrum must ultimately fall off faster than $|k_z|^{-3}$ (Bieber et al. 1988), and so we have chosen a -3 index for the dissipation range of our model spectrum as shown in equation (13). (Technically, a $|k_z|^{-3}$ power law is the limit of allowable dissipation range spectra but is itself marginally disallowed because it yields a logarithmic divergence of the mean square curl of the magnetic field. However, the distinction between a $|k_z|^{-3}$ power law and an incrementally steeper one is inconsequential for the present work. See Smith et al. 1990a for further discussion of the dissipation range.)

We emphasize that the model spectrum developed above is not proposed as a universal spectrum applicable to every individual cosmic-ray event. On the contrary, both the absolute level and spectral slope of observed interplanetary spectra are observed to undergo large variations, which should be taken into account when modeling individual events. Use of concurrent observed magnetic spectra can lead to good agreement between observed and theoretical mean free paths (Dröge et al. 1993), but it is observed in addition that large discrepancies remain for many other events (Wanner & Wibberenz 1993; Wanner et al. 1993). However, detailed event modeling is not our present objective. Rather, we offer the model spectrum given by equation (13) and illustrated in Figure 5 as an aid for discussing general properties of particle scattering in dynamical magnetic turbulence.

With both $P_{xx}(k_z, 0)$ and $\Gamma(k_z, t)$ specified, we can now compute the Eulerian frequency spectrum from equations (2) and (3) together with the inverse transform of equation (1). As shown in Figure 6, the damping and random sweeping models have similar Eulerian spectra except for angular frequencies (ω) above 1 s^{-1}, where the damping model approaches an ω^{-2} variation while the random sweeping model approaches ω^{-3}.

Also shown in Figure 6 are upper limits for the angular gyrofrequency (Ω) of protons and electrons in a 4.12 nT magnetic field. (The values of B_0 and V_A adopted here were determined by taking long-term averages of data recorded on NSSDC's "omnitape" compilation of 1 AU solar wind data; King 1989). In the relativistic regime, protons and electrons of a given rigidity have nearly the same gyrofrequency. As rigidity decreases, however, the electron gyrofrequency exceeds the proton gyrofrequency by an increasing amount, which ultimately reaches a factor of 1836 when both species are nonrelativistic, as shown by the limit lines in Figure 6. In light of equation (12) and the Eulerian spectra in Figure 6, this means that low- to intermediate-rigidity protons will experience a different rate of scattering through 90° pitch angle than electrons of the same rigidity. This is the source of the fundamental difference between proton and electron scattering, which we will now demonstrate in detail.

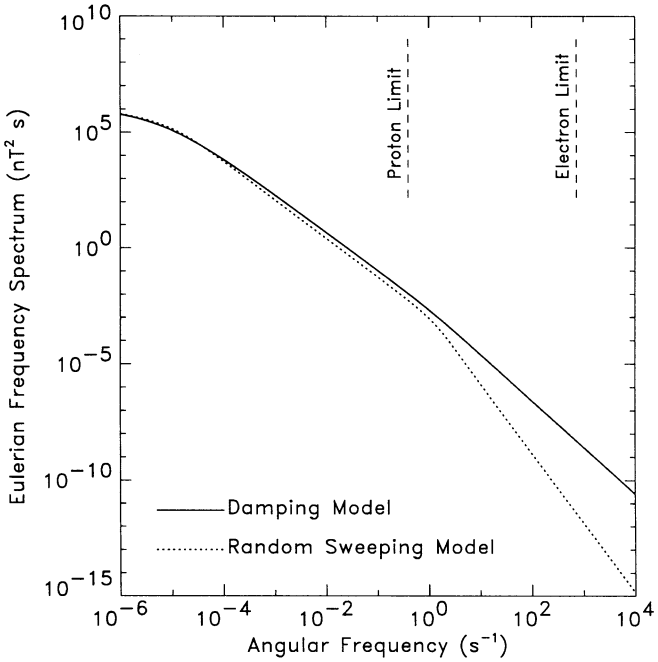

FIG. 6.—Eulerian frequency spectra for damping model (*solid line*) and random sweeping model (*dotted line*) of dynamical magnetic turbulence. Vertical dashed lines denote the angular gyrofrequency of nonrelativistic protons and electrons in the typical (4.12 nT) interplanetary magnetic field.

4.4. *Fokker-Planck Coefficient*

Figure 7 displays the Fokker-Planck coefficient for pitch-angle scattering in dynamical turbulence for 1 MV electrons and protons (*solid lines*). A fairly low rigidity was chosen in order to highlight the speed-dependent (or gyrofrequency-dependent) differences between electron and proton scattering. The computation employed the damping model of the dynamical correlation function with $\alpha = 1$ and incorporated a realistic dissipation range as described above. For comparison, the conventional slab result is also shown (*dashed lines*), using the magnetostatic limit of scattering and omitting the dissipation range. Results are normalized to the particle speed, since the mean free path scales inversely with $\Phi(\mu)/V$ as shown in equation (6). By virtue of this normalization, numerical values are identical for protons and electrons in the conventional slab model.

For 1 MV electrons with moderate pitch angles the scattering rate is nearly the same in the dynamical and conventional models. Below $\mu \approx 0.06$, however, the electrons are resonant with the dissipation range of the turbulence, and the scattering rate is strongly suppressed relative to the conventional model. Finally, below $\mu \approx 0.003$ the scattering rate approaches a constant value determined by the Eulerian frequency spectrum as shown in equation (12). Thus, dynamical effects produce finite

© American Astronomical Society • Provided by the NASA Astrophysics Data System

1994ApJ...420..294B

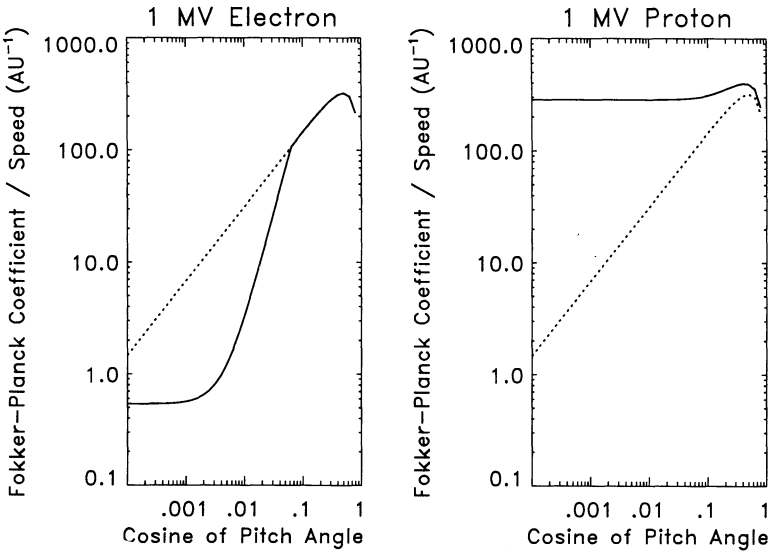

FIG. 7.—Fokker-Planck coefficient normalized to particle speed for 1 MV electrons (*left*) and protons (*right*) plotted against the cosine of the particle pitch angle. The solid line shows results derived here for the damping model of dynamical turbulence with slab geometry and a realistic dissipation range. The dotted line is the conventional quasi-linear theory result for a magnetostatic, dissipationless slab model.

scattering at 90° pitch angle, thereby avoiding the divergent mean free paths caused by the dissipation range in magnetostatic models (Bieber et al. 1988; Smith et al. 1990a). However, the dynamical effect is sufficiently small that the electron experiences much of the suppressed power (and suppressed scattering) associated with the dissipation range. The net result is a mean free path of 0.021 AU, which is significantly larger than the conventional slab result of 0.0057 AU.

For 1 MV protons the picture is quite different. As noted in connection with Figure 6, nonrelativistic protons have a much lower gyrofrequency than electrons of the same rigidity. As a result, scattering at 90° pitch angle is much stronger (when normalized to the particle speed as in Fig. 7) for 1 MV protons than for 1 MV electrons. In fact, the scattering is so strong that the dissipation range of the wavenumber spectrum is irrelevant, and dynamical effects dominate over ordinary resonant scattering through part of the inertial range as well. The net result is a mean free path of 0.0023 AU, which is smaller than the conventional slab result of 0.0057 AU.

The shape of the proton curve in Figure 7 suggests that we might try approximating the Fokker-Planck coefficient by $\Phi(\mu) \approx (1 - \mu^2)\Phi(0)$, with $\Phi(0)$ given by equation (12). According to equation (6) the mean free path is then $\lambda_{\|} \approx V/\Phi(0)$. This approximation overestimates the mean free path by about 50% for 1 MV protons, but it becomes increasingly accurate as rigidity decreases. In this regime the proton mean free path varies in direct proportion to the proton speed (or rigidity), and its magnitude is determined by the Eulerian frequency spectrum.

4.5. *Proton and Electron Mean Free Paths: Slab Geometry*

We come now to the key theoretical results of this work. Figure 8 displays proton (*dashed curve*) and electron (*solid curve*) mean free paths as a function of rigidity for scattering in dynamical turbulence with a realistic dissipation range. The computation employed the damping model of the dynamical correlation function with $\alpha = 1$. The conventional slab result (i.e., magnetostatic limit omitting the dissipation range) is shown for comparison (*dotted line*). We also depict (*shaded band*) the range of consensus mean free paths enunciated by Palmer (1982).

Use of the damping model in slab geometry does raise predicted low-energy electron mean free paths, but the amount of increase is insufficient to eliminate the problem of "too-small" theoretical mean free paths. From 1 to 100 MV predicted electron mean free paths are still a factor of ~ 5 below the midpoint of the Palmer consensus. On the other hand, the predicted rigidity variation of electron and proton mean free paths is significantly improved in comparison with predictions of the conventional slab model.

Notably, the model performs quite well in satisfying the *Helios* observational constraints described in § 3. Specifically, the proton mean free path increases monotonically in a manner similar to that predicted by the conventional slab model, and the mean free path of 1.4 MV electrons (0.020 AU) is close to that predicted for 187 MV protons (0.029 AU). The

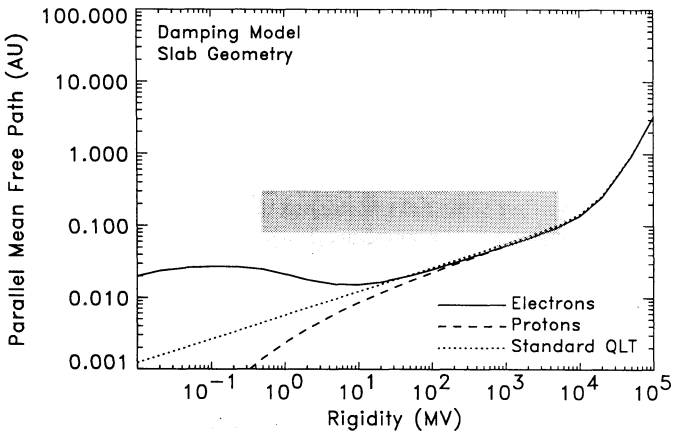

FIG. 8.—Proton (*dashed line*) and electron (*solid line*) mean free paths in the damping model of dynamical turbulence with pure slab geometry. The dotted line is the standard quasi-linear theory result for magnetostatic, dissipationless slab model. The shaded band is the observational consensus enunciated by Palmer (1982).

© American Astronomical Society • Provided by the NASA Astrophysics Data System

1994ApJ...420..294B

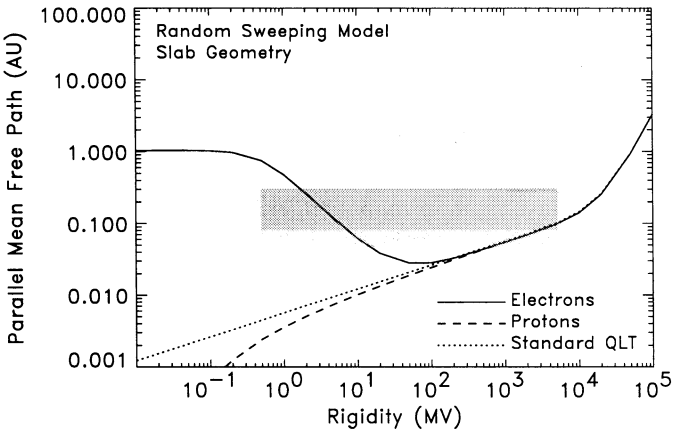

FIG. 9.—Proton (*dashed line*) and electron (*solid line*) mean free paths in the random sweeping model of dynamical turbulence with pure slab geometry. The dotted line is the standard quasi-linear theory result for a magnetostatic, dissipationless slab model. The shaded band is the observational consensus enunciated by Palmer (1982).

predicted ratio of 1.4 MV electron to 187 MV proton mean free paths is thus 0.69, as compared with a typical observed ratio of 0.56 and a prediction of 0.20 in the conventional slab model. For reasons discussed above in § 4.4, electron mean free paths are substantially larger than proton mean free paths at low to intermediate rigidities, but above ~50 MV both the proton and electron mean free paths approach the conventional slab result. Perhaps the most important deficiency of the damping model is the lack of an upturn in the electron curve at the lowest rigidities, as would seem to be required by observations of scatter-free electrons (Lin 1985).

Results for the random sweeping model of dynamical turbulence are presented in Figure 9. Both proton and electron mean free paths are increased relative to the damping model, an effect that is traced to the lower Eulerian frequency spectra obtained for random sweeping (Fig. 6). The most striking difference between the two models is the much deeper minimum in the electron curve for random sweeping. This model seems well able to account for scatter-free electrons at very low rigidities. However, the electron mean free path remains quite high at 1.4 MV, to the extent that 1.4 MV electrons have a substantially larger mean free path (0.362 AU) than 187 MV protons (0.030 AU), in disagreement with the *Helios* results of § 3.

4.6. *Proton and Electron Mean Free Paths: Composite Slab/Two-dimensional Geometry*

Both of the dynamical turbulence models discussed so far have employed pure slab geometry and have yielded mean free paths that fall well below the Palmer consensus band through at least part of the rigidity range considered. However, slab geometry is but one of a rich variety of turbulence geometries allowable under the most general axisymmetric description (Matthaeus & Smith 1981).

Of particular interest is the possibility that turbulence in space might be a composite of slab and two-dimensional geometries. Matthaeus, Goldstein, & Roberts (1990) have reviewed evidence from a variety of sources, including solar wind observations, that interplanetary magnetic turbulence may contain a "Strausslike" two-dimensional component (Strauss 1976; Montgomery 1982), for which both the turbulence wavevectors and the fluctuating magnetic field are perpendicular to the mean magnetic field. Such a two-dimensional component would contribute to the level of magnetic turbulence measured by a magnetometer but would not contribute to the ordinary resonant scattering of particles.

The theory of scattering in two-dimensional or composite slab/two-dimensional turbulence is considerably more complicated than for pure slab geometry. Mathematical details may be found in the Appendix, together with a discussion of our two-dimensional spectrum model. In the present subsection, we will focus on the results, to illustrate how turbulence geometry may provide the solution to the problem of "too-small" theoretical mean free paths. We employ a composite geometry comprised of 20% slab component and 80% two-dimensional component. Although a two-dimensional component comprising 80% of the turbulence may seem rather high, we are not aware of any observations that would rule this out.

Figure 10 presents the mean free path as a function of rigidity in composite slab/two-dimensional geometry. The electron mean free path now remains in or very near the Palmer consensus band, and the proton mean free path lies within the band through most of the regime of proton observations above 25 MV (see Fig. 1). At the higher rigidities the predicted mean free path is raised almost by a factor of 5 relative to pure slab geometry, in direct proportion to the amount by which the slab component of turbulence has been reduced. At lower rigidities, the mean free path is raised by substantially less than a factor of 5 because dynamical effects as well as ordinary resonant scattering play a role in determining the mean free path.

The composite model performs well in satisfying the *Helios* observational constraints. Proton mean free paths increase monotonically with rigidity, and the 1.4 MV electron mean free path (0.068 AU) is almost exactly half the 187 MV proton mean free path (0.137 AU). Once again the primary deficiency of the damping model is its inability to account for predominantly scatter-free electrons below 0.2 MV.

5. CONCLUSION

Standard quasi-linear theory (Jokipii 1966) conflicts with observation in two important ways. The first problem, which we will call the "magnitude problem," is simply that observed

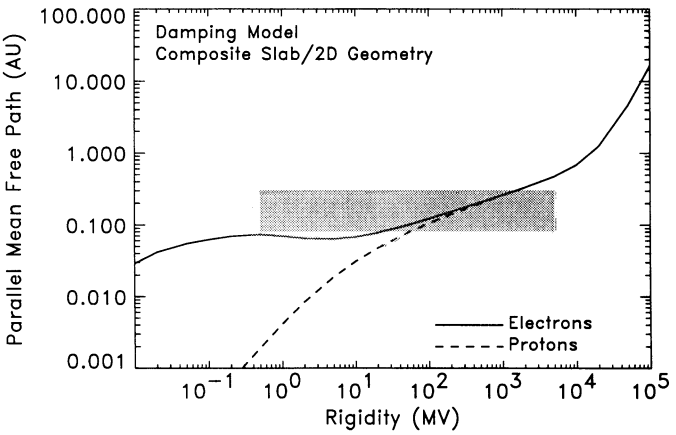

FIG. 10.—Proton (*dashed line*) and electron (*solid line*) mean free paths in the damping model of dynamical turbulence with composite slab/two-dimensional geometry. Slab and two-dimensional components are respectively 20% and 80% of the total fluctuating field. The shaded band is the observational consensus enunciated by Palmer (1982).

© American Astronomical Society • Provided by the NASA Astrophysics Data System

1994ApJ...420..294B

mean free paths are typically much larger than those predicted by the theory. The second problem, which we will call the "flatness problem," is that the rigidity dependence of observed mean free paths is nearly flat, or perhaps has a broad minimum, but the theory predicts monotonically increasing mean free paths. This, at least, is how the conflict between theory and observation was characterized by Palmer (1982) and how it is generally viewed today.

Based upon a critical reexamination of the Palmer consensus as well as new results from *Helios*, we suggest that the flatness problem actually exists only for cosmic-ray electrons. The observational database assembled by Palmer (and extended here in Fig. 1) is derived exclusively from electron observations below 25 MV. If these data points are omitted, the evidence for a flat rigidity dependence is not compelling. On the contrary, protons persistently exhibit monotonically increasing mean free paths from ~ 100 to ~ 300 MV when the mean free paths are derived from *Helios* multichannel observations in individual events. Owing to large event-to-event variability, however, this effect easily becomes obscured when data from many different events are presented together (Wanner & Wibberenz 1993).

At the same time, *Helios* data do support the reality of the flatness problem for electrons. In five of 11 events considered, 1.4 MV electrons had nearly the same mean free path as 187 MV protons, and a typical ratio (electrons to protons) is 0.56. We found no events with a ratio as small as the value (0.20) expected for the conventional slab model with a Kolmogorov inertial range. Taken together, the *Helios* results are still consistent with pure rigidity dependence of the mean free path, provided that the character of this dependence changes rather dramatically somewhere in the unobserved region between 1.4 and 100 MV. However, an alternative interpretation, fully consistent with observation, is that the proton and electron curves have bifurcated and are following different rigidity dependences at low to intermediate rigidities.

Such a bifurcation is a natural outcome of scattering theories that recognize the dynamical character of turbulence. It occurs because the scattering rate at and near 90° pitch angle is governed not by the usual resonance with the spectrum of spatial variations (i.e., the $\boldsymbol{k}$-space spectrum), but rather by resonance with the Eulerian frequency spectrum which represents dynamical aspects of the turbulence. This resonance occurs at the particle gyrofrequency, which produces a speed dependence or, equivalently, a mass dependence (beyond that inherent in rigidity dependence) in the scattering mean free path.

The wave model presented by Achatz et al. (1993a, b) also leads to differences between electrons and protons of the same rigidity. In this case the difference occurs because electrons and protons resonate with different parts of the spectrum when the warm plasma dispersion relation is used to determine the resonance condition. The wave model predicts a characteristic upturn of the electron mean free path at low rigidities, which is qualitatively similar to the results presented here in Figure 8 and 9. However, the model also predicts a very sharp upturn of the proton mean free path, which disagrees with the observations.

In contrast, both proton and electron mean free paths remain well behaved in the two different models of dynamical turbulence presented here. Both models predict a bifurcation of proton and electron mean free paths at ~ 50 MV, and both predict monotonically increasing proton mean free paths in accord with the *Helios* observations. The electron mean free path is roughly constant below 50 MV in the damping model of dynamical turbulence, which results in excellent agreement with the *Helios* observations. The random sweeping model, in contrast, exhibits a comparatively deep minimum in the rigidity dependence of the electron mean free path and is well suited for explaining the predominance of "scatter-free" electrons below 0.2 MV (Lin 1985).

Effects of dynamical turbulence can thus solve the flatness problem for electrons (which is all the observations really require), but the magnitude problem remains for both protons and electrons when pure slab geometry is assumed. Possibilities do exist for raising predicted mean free paths even within the confines of the slab model, for example, by decreasing the dissipation wavenumber (Bieber & Matthaeus 1991; Dröge et al. 1993), increasing the dissipation range steepness, or adopting large values of the cross-helicity (Dröge et al. 1993).

Alternatively, solution of the magnitude problem may require consideration of geometries other than the pure slab model. Motivated by recent suggestions that turbulence in the solar wind may be a composite of slab and two-dimensional geometries (Matthaeus et al. 1990), we computed the mean free path in such a composite geometry using the damping model of dynamical turbulence. Setting the two-dimensional component to 80% results in an electron mean free path that remains in or very near the Palmer consensus band throughout the defined rigidity range of the band. Proton mean free paths remain in or near the Palmer consensus band for rigidities above 50 MV, which is all the observations demand.

We thank Paul Evenson for useful discussions. This research was supported by NASA under grant NAGW-1637 and the Space Physics Theory Program and by NSF under grant ATM-9014806. W. H. M. was partially supported by NSF grant ATM-8913627. The Kiel group was partially supported by the Deutsche Forschungsgemeinschaft under Wi 259/9-1. Computing support was provided by the San Diego Supercomputer Center.

APPENDIX

PARTICLE SCATTERING IN TWO-DIMENSIONAL TURBULENCE

In order to discuss scattering in two-dimensional or composite slab/two-dimensional geometries, we generalize equation (2) to a three-dimensional power spectrum matrix in which k_z is replaced by the wavevector $\boldsymbol{k}$:

$$P_{ij}(\boldsymbol{k}, t) = P_{ij}^{(0)}(\boldsymbol{k})\Gamma(\boldsymbol{k}, t) . \tag{14}$$

© American Astronomical Society • Provided by the NASA Astrophysics Data System

1994ApJ...420..294B

For the damping model of two-dimensional turbulence, we assume $\Gamma = \exp(-\alpha k_\perp V_A |t|)$, where $k_\perp$ is the perpendicular (to the mean field) wavenumber. In the present work we consider only $\alpha = 1$. Taking the z-axis (denoted by tensor index 3) to correspond to the mean field direction, we define the magnetostatic limit of the spectrum as

$$P_{ij}^{(0)}(\boldsymbol{k}) = C\lambda \frac{g(k_\perp)}{k_\perp} \delta(k_z)\left(\delta_{ij} - \frac{k_i k_j}{k_\perp^2}\right), \tag{15}$$

for $i, j = 1, 2$, and $P_{ij}^{(0)} = 0$ if either i or $j = 3$. Here C and λ are parameters, δ_{ij} is the Kronecker symbol, and

$$g(k_\perp) = \begin{cases} (1 + k_\perp^2 \lambda^2)^{-5/6} & \text{for } k_\perp < k_d , \\ (1 + k_d^2 \lambda^2)^{-5/6}(k_\perp/k_d)^{-3} & \text{for } k_\perp \geq k_d . \end{cases} \tag{16}$$

Equation (15) describes a turbulence model for which both the wavevectors and the magnetic field fluctuations are perpendicular to the mean magnetic field. It can be shown that this power spectrum matrix has one of the allowed tensor forms of axisymmetric turbulence (Matthaeus & Smith 1981).

In two-dimensional turbulence, it is possible to define separate parallel and perpendicular reduced spectra:

$$P_\parallel(k_x) = \int_{-\infty}^{+\infty} dk_y \int_{-\infty}^{+\infty} dk_z \, P_{xx}^{(0)}(\boldsymbol{k}) , \tag{17}$$

$$P_\perp(k_x) = \int_{-\infty}^{+\infty} dk_y \int_{-\infty}^{+\infty} dk_z \, P_{yy}^{(0)}(\boldsymbol{k}) . \tag{18}$$

Note that the subscripts $\perp$ and $\parallel$ refer to the relative orientation between the matrix element under consideration (xx or yy in this instance) and the wavevector component that remains after reduction (k_x). Using the definitions of the two reduced spectra, it is possible to show that they are related by

$$P_\perp(k_x) = -k_x \frac{dP_\parallel}{dk_x} . \tag{19}$$

Figure 11 compares the parallel and perpendicular reduced spectra of the two-dimensional turbulence model with the reduced spectrum of the slab model described in § 4.3. For the two-dimensional model, the parameters C and λ were set to 1.91 nT^2 and 3.58×10^9 m, respectively. These values were selected to satisfy two conditions: (1) that the reduced perpendicular spectrum of the two-dimensional model be nearly identical to the reduced perpendicular spectrum of the slab model in the turbulence inertial range and (2) that the perpendicular correlation length of the two-dimensional model be the same as the perpendicular correlation length of the slab model (specifically, 3.4×10^9 m).

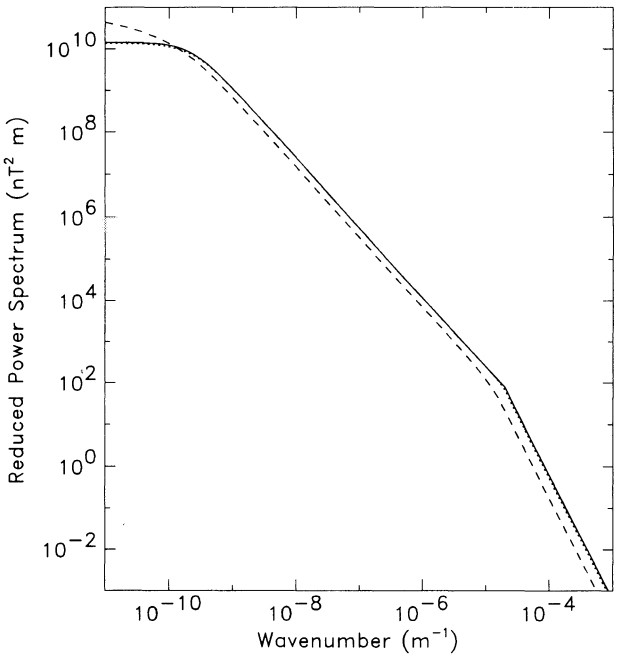

FIG. 11.—Reduced perpendicular power spectrum of the slab model (*solid line*) compared with the reduced perpendicular spectrum of the two-dimensional model (*dotted line*) and the reduced parallel spectrum of the two-dimensional model (*dashed line*). The two perpendicular spectra are nearly identical by design, hence the dotted line is mostly obscured by the solid line.

© American Astronomical Society • Provided by the NASA Astrophysics Data System

1994ApJ...420..294B

Methods for deriving the scattering rate in two-dimensional turbulence are similar to those described by Fisk et al. (1974) for isotropic turbulence. We will defer a detailed derivation to a forthcoming publication and present only the result here:

$$\Phi(\mu) = 4\pi C\lambda \frac{\Omega^4}{V^2 B_0^2} \sum_{n=1}^{\infty} \int_0^{\infty} \frac{dk_\perp}{k_\perp^2} g(k_\perp) D_n(k_\perp) n^2 [J_n(x)]^2 , \tag{20}$$

where $x = k_\perp V(1 - \mu^2)^{1/2}/\Omega$, and J_n is the nth-order Bessel function. The resonance function in two-dimensional turbulence depends on harmonic number n and is given by

$$D_n(k_\perp) = \frac{2\alpha k_\perp V_A}{\alpha^2 k_\perp^2 V_A^2 + n^2\Omega^2} . \tag{21}$$

We note finally that scattering rates for composite turbulence geometries can be computed by simple linear superposition. For example, the Fokker-Planck coefficient for the 80% two-dimensional model discussed in § 4.6 is simply the sum of 0.8 times equation (20) and 0.2 times equation (8).

REFERENCES

Achatz, U., Dröge, W., Schlickeiser, R., & Wibberenz, G. 1993a, J. Geophys. Res., 98, 13261
———. 1993b, Nucl. Phys. B, in press
Axford, W. I. 1965, Planet. Space Sci., 13, 1301
Beeck, J., & Wibberenz, G. 1986, ApJ, 311, 437
Beeck, J., Mason, G. M., Hamilton, D. C., Wibberenz, G., Kunow, H., Hovestadt, D., & Klecker, B. 1987, ApJ, 322, 1052
Bieber, J. W., & Burger, R. A. 1990, ApJ, 348, 597
Bieber, J. W., Chen, J., Matthaeus, W. H., Smith, C. W., & Pomerantz, M. A. 1993, J. Geophys. Res., 98, 3585
Bieber, J. W., Earl, J. A., Green, G., Kunow, H., Müller-Mellin, R., & Wibberenz, G. 1980, J. Geophys. Res., 85, 2313
Bieber, J. W., Evenson, P., & Matthaeus, W. H. 1987, Geophys. Res. Lett., 14, 864
Bieber, J. W., Evenson, P. A., & Pomerantz, M. A. 1986, J. Geophys. Res., 91, 8713
Bieber, J. W., & Matthaeus, W. H. 1991, Proc. 22d Int. Cosmic Ray Conf. (Dublin), 3, 248
———. 1992, in AIP Conf. Proc. 264, Particle Acceleration in Cosmic Plasmas, ed. G. P. Zank & T. K. Gaisser, (New York: AIP), 86
Bieber, J. W., & Pomerantz, M. A. 1983, Geophys. Res. Lett., 10, 920
Bieber, J. W., Smith, C. W., & Matthaeus, W. H. 1988, ApJ, 334, 470
Chen, J., & Bieber, J. W. 1993, ApJ, 405, 375
Chen, S., & Kraichnan, R. H. 1989, Phys. Fluids A, 1, 2019
Chenette, D. L. 1980, J. Geophys. Res., 85, 2243
Coroniti, F. V., Kennel, C. F., Scarf, F. L., & Smith, E. J. 1982, J. Geophys. Res., 87, 6029
Davila, J. M., & Scott, J. S. 1984, ApJ, 285, 400
Debrunner, H., & Lockwood, J. A. 1980, J. Geophys. Res., 85, 6853
Denskat, K. U., Beinroth, H. J., & Neubauer, F. M. 1983, J. Geophys., 54, 60
Dröge, W., Achatz, U., Wanner, W., Schlickeiser, R., & Wibberenz, G. 1993, ApJ, 407, L95
Dröge, W., Wibberenz, G., & Klecker, B. 1990, Proc. 21st Int. Cosmic Ray Conf. (Adelaide), 5, 187
Earl, J. A. 1974, ApJ, 193, 231
Evenson, P., Caldwell, J., Jordan, S., & Meyer, P. 1979, J. Geophys. Res., 84, 5361
Fisk, L. A., Goldstein, M. L., Klimas, A. J., & Sandri, G. 1974, ApJ, 190, 417
Ford, T., Palmer, I. D., & Sanders, R. 1977, J. Geophys. Res., 82, 4704
Goldstein, M. L. 1976, ApJ, 204, 900
Goldstein, M. L., Klimas, A. J., & Sandri, G. 1975, ApJ, 195, 787
Hamilton, D. C. 1977, J. Geophys. Res., 82, 2157
Hasselmann, K., & Wibberenz, G. 1968, Z. Geophys., 34, 353
———. 1970, ApJ, 162, 1049
Hedgecock, P. C. 1975, Sol. Phys., 42, 497
Jaekel, U., & Schlickeiser, R. 1992, J. Phys. G, Nucl. Part. Phys., 18, 1089
Jokipii, J. R. 1966, ApJ, 146, 480
Jones, F. C., Birmingham, T. J., & Kaiser, T. B. 1978, Phys. Fluid, 21, 347
Kallenrode, M.-B. 1993, J. Geophys. Res., in press
Kallenrode, M.-B., Wibberenz, G., & Hucke, S. 1992, ApJ, 394, 351
Kane, S. R., Evenson, P., & Meyer, P. 1985, ApJ, 299, L107
King, J. H. 1989, Interplanetary Medium Data Book, Suppl. 4, 1985–1988 (Rep. NSSDC/WDC-A-R&S 89-17; Greenbelt: NASA)
Krause, F., & Rädler, K.-H. 1980, Mean Field Electrodynamics and Dynamo Theory (New York: Pergamon)
Kunow, H., Wibberenz, G., Green, G., Müller-Mellin, R., & Kallenrode, M.-B. 1991, in Physics of the Inner Heliosphere II, ed. R. Schwenn & E. Marsch (New York: Springer), 243
Kunstmann, J. E. 1979, ApJ, 229, 812
Lee, M. A., & Völk, H. J. 1975, ApJ, 198, 485
Lin, R. P. 1970, J. Geophys. Res., 75, 2583
Lin, R. P. 1974, Space Sci. Rev., 16, 189
———. 1985, Sol. Phys., 100, 537
Lockwood, J. A., Debrunner, H., Flückiger, E., Neuenschwander, H., & Schubnell, M. 1982, J. Geophys. Res., 87, 4338
Mason, G. M., Ng, C. K., Klecker, B., & Green, G. 1989, ApJ, 339, 529
Ma Sung, L. S., & Earl, J. A. 1978, ApJ, 222, 1080
Matthaeus, W. H., Goldstein, M. L., & King, J. H. 1986, J. Geophys. Res., 91, 59
Matthaeus, W. H., Goldstein, M. L., & Roberts, D. A. 1990, J. Geophys. Res., 95, 20,673
Matthaeus, W. H., & Smith, C. W. 1981, Phys. Rev. A, 24, 2135
Matthaeus, W. H., & Zhou, Y. 1989, Phys. Fluids B, 1, 1929
McCarthy, J., & O'Gallagher, J. J. 1976, Geophys. Res. Lett., 3, 53
Moffatt, H. K. 1978, Magnetic Field Generation in Electrically Conducting Fluids (Cambridge: Cambridge Univ. Press)
Montgomery, D. 1982, Phys. Scripta T2/1, 83
Nelkin, M., & Tabor, M. 1990, Phys. Fluids A, 2, 81
Ng, C. K., & Wong, K.-Y. 1979, Proc. 16th Int. Cosmic Ray Conf. (Kyoto), 5, 252
Owens, A. J. 1974, ApJ, 191, 235
Palmer, I. D. 1982, Rev. Geophys. Space Phys., 20, 335
Palmer, I. D., Palmeira, R. A. R., & Allum, F. R. 1975, Sol. Phys., 40, 449
Palmer, I. D., Zwickl, R. D., Webber, W. R., & McDonald, F. B. 1978, J. Geophys Res., 83, 2461
Parker, E. N. 1965, Planet. Space Sci., 13, 9
Potter, D. W., Lin, R. P., & Anderson, K. A. 1980, ApJ, 236, L97
Reid, G. C. 1964, J. Geophys. Res., 69, 2659
Roelof, E. C. 1969, in Lectures in High Energy Astrophysics, ed. H. Ogelman & J. R. Wayland (NASA SP-199), 111
Ruffolo, D. 1991, ApJ, 382, 688
Sanada, T., & Shanmugasundaram, V. 1992, Phys. Fluids A, 4, 1245
Schlickeiser, R. 1988, J. Geophys. Res., 93, 2725
———. 1989, ApJ, 336, 264
Schlickeiser, R., & Achatz, U. 1993, J. Plasma Phys., 49, 63
Schlickeiser, R., Dung, R., & Jaekel, U. 1991, A&A, 242, L5
Schlüter, W. 1985, Ph.D. thesis, Universität Kiel
Schulze, B. M., Richter, A. K., & Wibberenz, G. 1977, Sol. Phys., 54, 207
Smart, D. F., Shea, M. A., Humble, J. E., & Tanskanen, P. J. 1979, Proc. 16th Int. Cosmic Ray Conf. (Kyoto), 5, 238
Smith, C. W., Bieber, J. W., & Matthaeus W. H. 1990a, ApJ, 363, 283
Smith, C. W., Matthaeus, W. H., & Ness, N. F. 1990b, Proc. 21st Int. Cosmic Ray Conf. (Adelaide), 5, 280
Strauss, H. R. 1976, Phys. Fluids, 19, 134
Tennekes, H. 1975, J. Fluid Mech., 67, 561
Valdés-Galicia, J. F., Wibberenz, G., Quenby, J. J., Moussas, C., Green, G., & Neubauer, F. M. 1988, Sol. Phys., 117, 135
Völk, H. J. 1975, Rev. Geophys. Space Phys., 13, 547
Wanner, W., & Wibberenz, G. 1991, Proc. 22d Int. Cosmic Ray Conf. (Dublin), 3, 217
———. 1993, J. Geophys. Res., 98, 3513
Wanner, W., Wibberenz, G., Jaekel, U., & Kallenrode, M.-B. 1993, Proc. 23d Int. Cosmic Ray Conf. (Calgary), 3, 234
Wibberenz, G., Hasselmann, K., & Hasselmann, D. 1970, Acta Phys. Acad. Sci. Hung., Suppl., 29, (No. 2), 37
Wibberenz, G., Kecskeméty, K., Kunow, H., Somogyi, A., Iwers, B., Logachev, Y. I., & Stolpovskii, V. G. 1989, Sol. Phys., 124, 353
Yakhot, V., Orszag, S. A., & She, Z. S. 1989, Phys. Fluids A, 1, 184
Zel'dovich, Y., Ruzmaikin, A., & Sokoloff, D. 1983, Magnetic Fields in Astrophysics (New York: Gordon & Breach)
Zwickl, R. D., & Webber, W. R. 1977, Sol. Phys., 54, 457
———. 1978, J. Geophys. Res., 83, 1157

© American Astronomical Society • Provided by the NASA Astrophysics Data System